

1 **Threonine phosphorylation regulates the molecular assembly and**
2 **signaling of EGFR in cooperation with membrane lipids**

3
4
5 Ryo Maeda¹, Hiroko Tamagaki-Asahina², Takeshi Sato², Masataka Yanagawa¹, and
6 Yasushi Sako^{1,3,*}

7
8 ¹Cellular Informatics Laboratory, RIKEN CPR, Wako, Saitama 351-0198, Japan; ²Kyoto
9 Pharmaceutical University, 5, Misasagi-cho, Yamashina, Kyoto, 607-8414, Japan;

10 ³CREST JST, 4-1-8, Honcho, Kawaguchi, 332-0012, Japan

11
12
13 *To whom correspondence should be addressed. E-mail: sako@riken.jp

14

15 **Abstract**

16 The cytoplasmic domain of the receptor tyrosine kinases (RTKs) plays roles as a
17 phosphorylation enzyme and a protein scaffold but the allocation of these two functions
18 is not fully understood. We here analyzed assembly of the transmembrane (TM)-
19 juxtamembrane (JM) region of EGFR, one of the best studied species of RTKs, by
20 combining single-pair FRET imaging and a nanodisc technique. The JM domain of EGFR
21 contains a threonine residue (Thr654) that is phosphorylated after ligand association. We
22 observed that the TM-JM peptides of EGFR form anionic lipid-induced dimers and
23 cholesterol-induced oligomers. The two forms involve distinct molecular interactions,
24 with a bias towards oligomer formation upon threonine phosphorylation. We further
25 analyzed the functions and oligomerization of whole EGFR molecules, with or without a
26 substitution of Thr654 to alanine, in living cells. The results suggested an autoregulatory
27 mechanism in which Thr654 phosphorylation causes a switch of the major function of
28 EGFR from kinase activation dimers to scaffolding oligomers.

29

30 **Introduction**

31 Epidermal growth factor receptor (EGFR) is an RTK responsible for cell proliferation and
32 differentiation (1, 2) and consists of five domains; an extracellular domain that interacts
33 with extracellular ligands, a single-pass transmembrane (TM) helix, a juxtamembrane
34 (JM) domain, a cytoplasmic kinase domain, and a C-terminal tail domain for interaction
35 with various cytoplasmic proteins (3, 4). Ligand association changes the conformation of
36 EGFR in its extracellular domain (5) and induces formation of an asymmetric dimer of
37 the intracellular kinase domains (6). This dimerization subsequently results in the
38 phosphorylation of tyrosine residues on the tail domain and the recruitment of
39 intracellular signal proteins such as GRB2 and PLC γ containing SH2 and/or PTB domains
40 (7). Although the atomic structures of most of the EGFR domains excluding the tail
41 domain have been elucidated individually (5, 6, 8-10), the overall architecture of this
42 protein has not yet been revealed, leaving several unanswered questions about the
43 molecular mechanisms underlying its functions. The correlation between the arrangement
44 of EGFR molecules and their function is therefore still controversial, e.g., it has long been
45 established that the dimerization of EGFR is necessary and sufficient for kinase activation
46 (11), whereas several studies have reported the importance of higher-order
47 oligomerization for EGFR-mediated signal transduction (12-14).

48 The TM helix and the JM domain (TM-JM) of EGFR play important roles in the
49 conformational coupling of ligand binding to its activation and oligomerization (9, 11,
50 15). Previous NMR studies and molecular dynamics simulations have suggested that the
51 TM domain forms an α -helix dimer that undergoes a change in the interaction between
52 GXXXG motives (9, 16, 17) following the ligand association with its extracellular
53 domains (17, 18). This information regarding conformational changes in the TM dimer is
54 then transmitted to the JM domain which comprises a JM-A (N-terminal half) region that
55 can form an antiparallel helix dimer, and a JM-B (C-terminal half) region which makes
56 intramolecular contact with the kinase domain (11). Both these JM regions contribute to
57 the stable formation of an asymmetric kinase dimer conformation, which is crucial for
58 kinase activation. The JM-A domain is rich in Lys and Arg residues, several of which are
59 thought to interact with anionic lipid molecules of the plasma membrane and promote
60 antiparallel dimer formation (19-21). In addition to the phospholipid species, cholesterol
61 is a major component of the plasma membrane, mainly distributed as lipid rafts and
62 caveolae, and has been implicated in the regulation of membrane fluidity and receptor
63 function. Previous studies have shown that EGFR molecules are clustered in lipid rafts
64 (14, 22), suggesting an interaction with cholesterol. Of note in this regard, it has been
65 reported that the depletion of cholesterol induces various effects on EGFR signaling,

66 also this remains controversial (23-25). Another important factor in the regulation of
67 EGFR through the TM-JM is the phosphorylation of Thr654 at the JM-A domain.
68 Although Thr phosphorylation is known to be involved in EGFR deactivation, the precise
69 mechanism of this is still elusive (26).

70 In our present study, by combining single-pair FRET measurements and
71 nanodisc technology, we studied how the functions of anionic lipids, cholesterol, and
72 EGFR Thr654 phosphorylation (pT654) are orchestrated to achieve the regulation of
73 dimerization and/or oligomerization of EGFR. We previously reported that anionic lipids
74 cause the dimerization of JM domains, and that pT654 together with acidic lipids induces
75 the dissociation of the EGFR dimer (20). In this current study, we report that both the TM
76 and JM protomers of EGFR are positioned closer to each other in the presence of
77 cholesterol than in the EGFR dimers promoted by anionic lipids. Furthermore, we found
78 that TM-JM peptides were oligomerized in cholesterol containing membranes, which was
79 promoted by pT654. Finally, in living cells expressing whole EGFR molecules, we
80 observed differential functional roles and oligomerization states that are dependent on the
81 pT654 levels. Our recent study also shows that EGF-induced oligomerization of EGFR
82 depends on the cholesterol density in the plasma membrane (27). These results suggest
83 that the membrane cholesterol and pT654 cooperatively shift the EGFR function from the
84 kinase dimer to the scaffold oligomer.

85

86 **Results**

87 **Incorporation of TM-JM peptides into nanodiscs**

88 Synthesized peptides of the TM-JM region of EGFR were prepared and labeled with a
89 fluorophore Cy3 or Cy5 at the N-terminus (TM terminal region) or C-terminus (JM
90 terminal region), respectively (Fig. 1a). The peptides were reconstituted into nanodisc
91 structures with membrane scaffold proteins (MSPs) and lipid molecules (Fig. 1b, c).
92 Mixtures of POPC (PC), POPS (PS), and cholesterol were used for reconstruction (Fig.
93 1d). The nanodiscs containing cholesterol showed two peaks following size exclusion gel
94 chromatography, one of which had a smaller disc size relative to that without cholesterol
95 (Fig. 1e). To avoid the effects of disc size, we collected and used nanodiscs involved in
96 the first peak fraction which had a similar size without cholesterol. This fraction was
97 composed of the same ratio of lipids as used in the preparation (Fig. 1f). Fractions of PS
98 (inner leaflet) and cholesterol (inner and outer leaflets) mimicked those in the plasma
99 membrane. Synthesized TM-JM peptides with pT654 were also reconstituted into
100 nanodiscs. The nanodisc construction was examined under a transmission electron
101 microscope (Fig. 1g). In total, 16 types of nanodiscs were applied to subsequent single-
102 molecule measurements.

103

104 **TM-TM interaction in the EGFR dimer**

105 Nanodiscs containing Cy3 and Cy5-labeled peptides were immobilized onto glass
106 surfaces and illuminated with a 532-nm laser for Cy3 excitation. A portion of the
107 fluorescent spots contained Cy5 fluorescence derived from the occurrence of FRET (Fig.
108 2a, b). Based on the fluorescence intensity, we selected nanodiscs containing one Cy3-
109 and one Cy5-labeled peptide and calculated the FRET efficiency, E_{FRET} (Fig. 2c).

110 We first examined the interactions between the N-terminal regions of the TM
111 domains (Fig. 3). When Thr654 was not phosphorylated and the membrane contained
112 only PC as lipid species, E_{FRET} distributed with a peak at a relatively high (> 0.90 ; Table
113 D) value (Fig. 3a), indicating close proximity of the two TM domains. There may be
114 additional stable structures between the TM domains, as suggested by the small peaks and
115 shoulders in the E_{FRET} distribution. The addition of anionic lipid PS caused few effects,
116 i.e., the TM dimers were maintained as the major structure (Fig. 3b). Peptides with pT654
117 slightly decreased the major peak positions of the E_{FRET} distributions in the PC or PC/PS
118 membranes (Fig. 3e, f). The smooth distribution of the pT654 peptides suggested that
119 pThr654 had homogenized possible substructures of the TM dimers of non-
120 phosphorylated peptides. PS had little effect on the TM-TM interactions regardless of the
121 Thr654 phosphorylation. The presence of cholesterol in the membrane concentrated the

122 distributions to a high E_{FRET} (> 0.95) region (Fig. 3c, g, h), indicating that the N-terminal
123 regions of TM-TM dimers were positioned in extremely close proximity. Although the
124 peak position was similar in PC and PC/cholesterol membranes (Fig 3a, c; Table I), the
125 distribution in PC/cholesterol membrane was more accumulated at the peak position. It
126 also should be noted that the accumulation at a high E_{FRET} region was a remarkable
127 observation for pT654 peptides. Thus, pT654 and the presence of membrane cholesterol
128 decreased the distance between the two N-termini of the TM domains in cooperation. PS
129 competed with cholesterol when Thr654 was non-phosphorylated (Fig. 3d).

130

131 **JM-JM interaction in the EGFR dimer**

132 To examine the effects of lipid species and pT654 on JM-JM interaction, E_{FRET}
133 distributions were determined under the C-terminus labeling (Fig. 4). In PC membrane,
134 E_{FRET} was broadly distributed with a peak around 0.81 (Fig. 4a; Table I). It is plausible
135 that the JM-A dimers are fluctuating between minor dissociation and major association
136 states. In the PC/PS membrane, the peak fraction was increased, indicating that PS
137 stabilized the JM-A dimer conformation (Fig. 4b). pT654 increased the low FRET
138 fraction in the PC/PS membrane (Fig. 4f) but showed little effect in the PC membrane
139 (Fig. 4e). These results confirmed the results of our previous study (20). Cholesterol
140 moved the E_{FRET} peak between non-phosphorylated peptides to higher values (0.93–0.94)
141 regardless of whether it was a PC or PC/PS membrane (Fig. 4c, d), i.e., cholesterol forced
142 the C-termini of the JM-A domains to position closer.

143 The mixed effects of cholesterol and pT654 on the JM-JM interaction were
144 further examined. In the PC membrane (Fig. 4g), cholesterol increased the high FRET
145 population to a comparable level to those shown for non-phosphorylated peptides.
146 Cholesterol in the PC/PS membrane (Fig. 4h) reversed the E_{FRET} distribution seen in the
147 PC/PS membrane without cholesterol (Fig. 4f) to that observed in the PC membrane (Fig.
148 4e) i.e. minor low FRET and major high FRET states in the PC/PS/cholesterol membrane.
149 However, it should be noted that the E_{FRET} values were not as large as those found in other
150 conditions with cholesterol (Fig. 4c, d, g), i.e., the cholesterol effect on JM-JM interaction
151 was partially diminished by the coexistence of PS and pThr654. Overall, our data showed
152 that cholesterol increased the proximity between the C-terminus of JM domains in PC
153 and PC/PS membranes, and that this effect overrode that of pThr654 in the PC/PS
154 membrane.

155

156 **Higher-order oligomerization of TM-JM peptides**

157 We speculated that the accumulation of EGFR in lipid rafts, which has been reported in

158 previous studies, could be an effect of cholesterol in the raft membrane and examined the
159 assembly of TM-JM peptides in the nanodiscs, collecting images of fluorescent spots
160 containing only Cy3-labeled peptides to avoid interference from the effects of FRET
161 occurring between Cy3 and Cy5. Figure 5 displays the fluorescence intensity histograms
162 of C-terminus-labeled TM-JM peptides in nanodiscs containing or not-containing
163 cholesterol. Cholesterol shifted the histograms toward higher intensities for the pT654
164 peptides (Fig. 5b, d), suggesting a cooperative effect of cholesterol and Thr
165 phosphorylation to induce higher-order assembly of the TM-JM peptides.

166

167 **Assembly of TM regions**

168 For analysis of the interactions between more than two TM or JM domains in the
169 assembled structures at the N-terminus, images of fluorescent spots containing two Cy3-
170 labeled peptides and one Cy5-labeled peptide were collected based on their 2-color
171 fluorescence trajectories (Fig. 6a). These nanodiscs showed a variety of Cy3 donor
172 fluorescence intensities before Cy5 photobleaching indicating that the three peptides
173 interacted diversely. We constructed maximum fluorescence intensity histograms in the
174 Cy3 donor channel before and after Cy5 acceptor photobleaching for inference of the
175 interactions between three TM domains (Fig. 6b–i). In all conditions other than non-
176 phosphorylated peptides in the PC/PS membrane, Cy3 distributions after Cy5
177 photobleaching (red) peaked at the fluorescence intensity of ~100 (in arbitrary units),
178 which was smaller than that observed for the C-terminal-labeled peptides (~150; Fig. 7b–
179 i). This result must have been caused by homo-FRET (self-quenching) between two N-
180 terminal labeled Cy3 peptides. Together with the very small intensity peaks prior to Cy5
181 photobleaching (blue), these distributions suggested that TM regions of the three peptides
182 (two of them were randomly labeled with Cy3) were oligomerized in very close proximity
183 to each other in the major configuration (trimer; Fig. 6j).

184 For non-phosphorylated peptides in the PC/PS membrane however (Fig. 6c), the
185 Cy3 intensity histogram after Cy5 photobleaching (red) had a peak intensity at ~150,
186 indicating that two Cy3-labeled peptides in the major population were positioned
187 separately. In addition, the low intensity shoulder in this distribution indicated the
188 presence of proximate dimers (and trimers). Taken together, these distributions suggested
189 that N-terminal regions of three non-phosphorylated peptides have a stronger tendency to
190 arrange as one dimer and one monomer in the PC/PS membrane than any other condition.
191 A similar dimer + monomer arrangement might be contained in the distributions under
192 other conditions as a minor fraction. Consistent with this suggestion, for the non-
193 phosphorylated peptides in PC/PS membrane before Cy5 photobleaching (Fig. 6c, blue),

194 a homo-FRET fraction (~ 100 ; with a low E_{FRET} to Cy5) was evident compared to other
195 conditions. It should be noted that the ability of PS to promote the dimer + monomer
196 arrangement was diminished for pT654 peptides (Fig. 6g). Cholesterol also reduced this
197 effect of PS even for non-phosphorylated peptides (Fig. 6e). As observed in the earlier
198 analysis of the TM-JM peptide dimer (Fig. 3), the effects of PS and cholesterol were
199 competitive.

200

201 **Assembly of JM regions**

202 We constructed Cy3 fluorescence intensity histograms of two Cy3 and one Cy5 peptide
203 with C-terminal-labeling in single nanodiscs in order to analyze the interactions between
204 three JM domains (Fig. 7). The distributions of the Cy3 fluorescence after Cy5
205 photobleaching (red) were similar under all conditions, exhibiting a single peak at ~ 150 ,
206 which was the fluorescence intensity of the two Cy3 molecules without strong
207 interactions to induce homo-FRET. Both the trimer and dimer + monomer arrangements
208 are possible if we assume that the three molecules in the trimer and two molecules in the
209 dimer are not so close that they will induce homo FRET (Fig. 7j).

210 Prior to Cy5 photobleaching (blue), the distribution peaks were observed in the
211 region of small Cy3 intensities indicating the proximity of both Cy3 molecules with Cy5
212 to induce high E_{FRET} , as observed between two molecules in a nanodisc (Fig. 4), i.e., the
213 formation of a JM trimer. An accumulation in the low intensity peak fraction was very
214 evident for non-phosphorylated peptides in the membranes containing cholesterol (Fig.
215 7d, e). On the other hand, fractions at the intensities similar to those observed after Cy5
216 photobleaching were significant for pT654 peptides in the membrane without cholesterol
217 (Fig. 7f, g). In general, pT654 peptides exhibited higher fluorescence intensity compared
218 to non-phosphorylated peptides in the corresponding membrane lipid compositions. One
219 possible explanation is that the fraction of high Cy3 intensity before Cy5 photobleaching
220 represents a Cy3 dimer in the dimer + monomer arrangement of three peptides (Fig. 7j).
221 Another possibility is that it was caused by an increased distance between three JM
222 domains in trimers, resulting from Thr phosphorylation to reduce E_{FRET} (Fig. 7j top
223 middle). These two arrangements could potentially coexist.

224 Considering the possible arrangement for the TM and JM regions of three TM-
225 JM peptides together (Figs. 6 and 7), we conclude that cholesterol induces the closely
226 proximate oligomerization of three JM domains of non-phosphorylated peptides whereas
227 PS preferentially causes a dimer + monomer arrangement, and the Thr phosphorylation
228 disrupts the JM dimer and facilitates oligomerization of peptides with separated JM
229 domains in the presence of cholesterol (Fig. 8). Because of the limitation of FRET

230 measurement, we could not distinguish whether the peptides in the oligomers directly
231 interacted or not.

232

233 **Effect of Thr phosphorylation on the Tyr phosphorylation of EGFR**

234 Our single-molecule structural analysis suggested that pT654 is a key regulator of the
235 molecular assembly of EGFR, which may affect its functions. We examined this
236 possibility in living cells. It is known that PKC activation under EGF signaling induces
237 pT654 in EGFR. This process has been thought to be a negative feedback pathway in the
238 EGFR system. We expressed a wild type (wt) or T654A mutant EGFR in CHO-K1 cells,
239 which have no intrinsic expression of EGFR. An increase in pT654 was observed for wt
240 EGFR after EGF stimulation, and treatment of these cells with phorbol-12-myristate 13-
241 acetate (PMA), a PKC activator, caused stronger phosphorylation of Thr654 regardless
242 of EGF stimulation (Fig. 9a). Application of a saturation amount (100 ng/ml) of EGF to
243 the culture medium induced phosphorylation of Tyr1068 (pY1068) of both the wt and
244 T654A mutant EGFR proteins (Fig. 9b). pY1068 is a major association site on EGFR for
245 the adaptor protein GRB2 and its levels after EGF stimulation were significantly
246 increased by the T654A mutation compared to wt, as expected from the negative effect of
247 pT654. Whereas, pretreatment with PMA decreased the pY1068 level in both the wt and
248 T654A mutant EGFR (Fig. 9c). The PMA-induced decrease in pY1068 for the wt protein
249 could be a negative effect of increased pT654, but the similar result with the T654A
250 mutant suggests that PMA has indirect effects independent of pT654.

251

252 **Single-molecule imaging of the clustering and movement of EGFR**

253 We expressed EGFR (wt and T654A) fused with GFP in CHO-K1 cells and, by using
254 single-molecule imaging, detected cluster size distributions and lateral diffusion
255 movements of EGFR molecules in the plasma membrane (Fig. 10a). Clustering of EGFR
256 was measured as the fluorescence intensity distribution of EGFR spots, and the lateral
257 diffusion movements were measured as the increase in the mean square displacement
258 (MSD) of the spots with time. Both measurements were performed before and after 10
259 min of EGF application to the medium. Application of EGF to the medium induced
260 clustering and immobilization of wt EGFR as we have reported previously(14, 28). The
261 distributions of EGFR cluster size suggest formation of oligomers containing up to more
262 than 10 molecules (Fig. 10b). The convex shapes of MSD curve with time indicate
263 subdiffusion of EGFR molecules (Fig. 10c).

264 Even in the absence of EGF, PMA treatment of cells increased fractions of
265 higher-order wt EGFR oligomers (Fig. 10b left), though diffusion movements were hardly

266 affected (Fig. 10c left). This oligomerization was not as strong as that induced by EGF in
267 the absence of PMA, and application of EGF to the PMA treated cells did not induce
268 further oligomerization at least up to 10 min but significantly decreased mobility. While
269 in cells without PMA treatment, application of EGF induced strong oligomerization and
270 immobilized wt EGFR. For T654A mutant, PMA treatment hardly affected both
271 oligomerization (Fig. 10b right) and movements (Fig. 10c right) in the absence of EGF.
272 EGF induced strong oligomerization and immobilization of T654A mutant independent
273 of PMA treatment. The effects of PMA to induce EGFR oligomerization that was
274 dependent on Thr654 were consistent with pT654-induced oligomerization of TM-JM
275 peptides in nanodiscs.

276 In summary, single-molecule measurements suggest three states of EGFR
277 oligomerization depends on pT654 and EGF association (Fig. 10d). PMA treatment of wt
278 EGFR but not T654A mutant induced a medial level of oligomerization, which could be
279 stabilized by pT654. Strong oligomerization observed under the weak pT654 level in wt
280 EGFR and no pT654 in T654A mutant was caused by a distinct mechanism of pT654. On
281 the other hand, it is possible that immobilization of EGFR relates with its tyrosine
282 phosphorylation levels as we have observed previously (29). The EGF-induced
283 immobilization in the presence of PMA was more evident in T654A mutant in which
284 pY1068 level was higher than that in wt EGFR (Fig. 9), and PMA treatment decreased
285 immobilization and pY1068 in wt EGFR.

286

287 **Interaction of EGFR with GRB2**

288 We finally measured the interaction of EGFR with GRB2 in living cells using a split
289 luciferase (NanoBiT) assay, in which the C-terminus of EGFR and the N-terminus of
290 GRB2 were conjugated with the large BiT (LgBiT) and the small BiT (SmBiT) of
291 NanoLuc luciferase (30), respectively. The association of EGFR and GRB2 promoted the
292 formation of active luciferase to produce chemiluminescence emission (Fig. 11a). In the
293 timecourses of the NanoBiT signal increases after EGF treatment of cells expressing the
294 wt or T654A mutant EGFR (Fig. 11b), the maximum intensities indicated a dose
295 dependent response to the EGF concentration in the medium (Fig. 11b, c). The maximum
296 intensity was significantly increased after pretreatment with PMA in cells expressing wt
297 EGFR, despite the fact that the pY1068 level was reduced after the PMA treatment (Fig.
298 9c). This effect of PMA was not observed to any extent with the T654A mutant, and the
299 GRB2 association was not increased by this mutation in the absence of PMA, even though
300 the pY1068 level after EGF stimulation was significantly increased in the mutant (Fig.
301 9c). The increase in GRB2 association observed for wt EGFR after PMA treatment was

302 not likely to be an indirect effect of PMA because it was not observed for the T654A
303 mutant, in which the pY1068 level was also affected by PMA. These results suggest that
304 pT654 promotes the formation of a GRB2 recognition state for EGFR, and that the
305 inhibition of Thr654 phosphorylation prevents a GRB2-EGFR association in spite of
306 enhanced Tyr1068 phosphorylation.
307

308 Discussion

309 We have here studied the dimerization and oligomerization of EGFR molecules by
310 reconstituting its TM-JM peptides into nanodiscs. As expected from the positively
311 charged JM-A sequence and accumulation of EGFR in the raft membrane, PS and
312 cholesterol affect the molecular assembly of the TM-JM peptides. Interestingly, these two
313 lipid species each function in a specific fashion i.e. the E_{FRET} distributions between the
314 two TM-JM peptides in the nanodiscs suggested that PS facilitates JM dimerization, while
315 cholesterol induces closer positioning of both the TM and JM domains (Figs. 3 and 4). In
316 addition, cholesterol promoted the oligomeric assembly of TM-JM peptides (Figs. 6 and
317 7). We herein propose schematic models for the formation of the EGFR TM-JM dimers
318 and trimers under various conditions of lipid exposure and Thr654 phosphorylation (Fig.
319 8), in which PS and cholesterol exert competitive effects on dimerization and
320 oligomerization, and pT654 disrupts the PS-induced JM dimer, thus promoting
321 oligomerization of the peptides.

322 It should be noted that the E_{FRET} distribution was broad in every one of our
323 observations in this present study, especially between JM domains, indicating multiple
324 configurations coexisting under each condition. Non-phosphorylated peptide dimers
325 showed a peak at around $E_{FRET} > 0.90$ and > 0.81 both for N- and C-terminus labeling,
326 respectively. We can attribute this configuration to that suggested in a previous NMR
327 study, in which two JM domains form an anti-parallel helix dimer (9). PS stabilized this
328 configuration probably at the JM side of the non-phosphorylated peptide. Acidic lipids
329 are known to interact with the positively charged JM-A domain (19, 31) whereas
330 cholesterol induced more proximation of the two peptides at the both N- and C-termini in
331 the major configuration (E_{FRET} 0.95 and 0.93), which must be distinct from the
332 arrangement containing antiparallel JM helices (Fig. 8). If the TM-JM domains of whole
333 EGFR dimer adopt similar configurations as suggested for the TM-JM peptides in the
334 nanodiscs, the arrangement of two kinase domains indicates namely, the kinase activity
335 would be affected by the lipid composition and by pT654 (Fig. 11d).

336 Cholesterol was found in our current analysis to increase the population of
337 nanodiscs containing three TM-JM peptides with pT654 (Fig. 5). The fluorescence
338 intensity distributions of the two Cy3 probes among the three peptides in the presence of
339 cholesterol suggested that a close trimer was the major configuration (Figs. 6 and 7). The
340 cholesterol-induced oligomerization of TM peptides with a short JM region (to T654) of
341 EGFR in liposomes has been reported previously from NMR analysis (32). In that report
342 however, pT654 in the peptide showed no obvious effect on the oligomerization in PC
343 and PC/cholesterol liposomes (without any acidic lipids), consistent with our current and

344 previous results indicating interplay of acidic lipids and pT654. The induction of
345 oligomerization seems to be a general effect of cholesterol upon α -helix peptides in lipid
346 bilayers (33). Our result does not necessarily mean trimerization in the physiological
347 conditions but reflects a tendency of oligomerization. We picked up trimers in the analysis
348 to avoid complexity in the interactions between more than three molecules. While in the
349 PC/PS membrane without cholesterol (Figs. 6 and 7), the probability to adopt a one dimer
350 + one monomer configuration seems to be increased for the non-phosphorylated peptides,
351 likely because peptides have difficulty forming trimers when containing the anti-parallel
352 helix JM dimer, the pT654 event appears to dissociate the JM dimer to help in the
353 formation of the close trimer especially in the presence of cholesterol. If this assumption
354 is correct, oligomer formation will be inhibitory for EGFR kinase activity. Our observed
355 increases in the pY1068 level in the T654A mutant of EGFR (Fig. 9) support this
356 possibility.

357 Recently, we studied the effects of cholesterol depletion on EGF signaling under
358 the same experimental condition as used in this study (27). Treatment of cells with
359 methyl- β -cyclodextrin increased the fraction of preformed EGFR dimers and induced
360 hyperphosphorylation of Y1068 and Y1173 of EGFR upon EGF stimulation.
361 Nevertheless, cholesterol depletion diminished reactions downstream of EGFR
362 autophosphorylation, including the translocation of GRB2 to the cell surface and
363 phosphorylations of SHC, AKT, and ERK. It also strongly inhibited the EGF-induced
364 clustering of EGFR over dimers. These observations are consistent with those of the
365 current study, suggesting biphasic functions of membrane cholesterol on the EGF
366 signaling. Cholesterol inhibits EGFR dimerization for kinase activation but promotes
367 oligomerization of the (relatively small amount of) tyrosine-phosphorylated EGFR to
368 enhance signaling to the downstream molecules.

369 The antiparallel helix dimer of JM is thought to facilitate asymmetric interaction
370 between the kinase domains of EGFR, and hence its activation, in order to phosphorylate
371 tyrosine residues in the C-tail (11, 34). This tyrosine phosphorylation results in the
372 recruitment of PKC and other threonine kinases from the cytoplasm to the EGFR
373 molecules for the phosphorylation of Thr654, which is known to negatively regulate
374 EGFR signaling (26, 35). Our previous results suggested that the mechanism underlying
375 this negative effect of pT654 is the dissociation of JM dimers in the presence of acidic
376 lipids (20). At the same time, pT654 might induce the oligomerization of EGFR in the
377 presence of cholesterol. Supporting this possibility, our current single-molecule imaging
378 in living cells revealed the oligomerization of unliganded wt EGFR after PMA treatment,
379 which induced pT654 (Fig. 10). In the unliganded condition, the extracellular domains of

380 EGFR are thought to prevent the JM dimerization for kinase activation (9, 36). Clustering
381 of EGFR is also prevented largely in the unliganded condition. However, probably due to
382 the structural fluctuation, a small part of the unliganded EGFR oligomerized (27). pT654
383 (PMA) stabilized the unliganded oligomers possibly destructing the JM antiparallel
384 dimers.

385 We previously reported that oligomers of EGFR formed after cell stimulation
386 with EGF function as the major signal transduction sites for GRB2, where the dissociation
387 rate constant with GRB2 was reduced increasing the affinity between single-molecules
388 of EGFR and GRB2 (14). In addition, our current analyses found an increase in the wt
389 EGFR/GRB2 association following PMA treatment (Fig. 11). We speculate that after the
390 initial Tyr phosphorylation, successive Thr phosphorylation reduces Tyr kinase activity
391 of EGFR but enhances the formation of signal transduction oligomer in the medium
392 immobilized and oligomerized state of EGFR molecules (Fig. 10d). Further
393 immobilization and oligomerization were found in our current experiments to be induced
394 by EGF in the absence of PMA for wt EGFR and with or without PMA for the T654A
395 mutant. This process might include EGFR molecules accumulated into the clathrin coated
396 pits (37) and be independent of pT654. In the previous report (38), ERK activation was
397 reduced by the Thr654/669 of EGFR to Ala substitution suggesting only negative effects
398 of Thr654, however, oligomerization of EGFR was not observed in this report. In addition,
399 because tyrosine phosphorylation is a prerequisite for EGFR signaling, strong inhibition
400 of the kinase activation will prevent the downstream signaling even after the
401 oligomerization of EGFR. In our experimental condition, even though pT654 was
402 inhibitory for EGFR kinase activity, it promoted signal transduction downstream.

403 Based on our present results, we propose a model of EGFR signaling regulated
404 by membrane lipids and Thr654 phosphorylation (Fig. 11d). The signal transduction
405 mediated by EGFR is a complex multi-step process. Conformational changes in the
406 extracellular domain of EGFR upon ligand association allow JM domains to form anti-
407 parallel JM helix dimers and asymmetric kinase domain dimers(11, 34). This is the
408 activation process for EGFR kinase, in which acidic membrane lipids and cholesterol play
409 stimulative and inhibitory roles, respectively (20, 27). Tyrosine phosphorylation in the
410 kinase-active EGFR dimers recruits PKC from the cytoplasm (39). The association of
411 PLC γ to the EGFR phosphotyrosine for the degradation of PIP $_2$ is involved in this process.
412 PKC then phosphorylates Thr654 (40), which dissociates anti-parallel JM dimers in the
413 presence of remaining acidic lipids and supports the oligomerization of EGFR in the
414 presence of cholesterol, especially after the removal of acidic lipids around the EGFR
415 molecules. The cholesterol-induced oligomer of EGFR is a major site of interaction with

416 cytoplasmic proteins including GRB2 (14). Thus, a major function of EGFR is shifted
417 from a kinase for self-activation to a scaffold for signal transduction. Thr654
418 phosphorylation is a key step underlying this role change of EGFR and is not merely an
419 inactivating mechanism. The degradation of PIP₂, a major anionic lipid in the inner leaflet
420 of the plasma membrane, may support this role change. Importantly, both Thr654
421 phosphorylation and PIP₂ degradation are caused by the kinase activation of EGFR.
422 Hence, this represents an ingenious autoregulatory process involving membrane proteins
423 and lipids.
424

425 **Materials and Methods**

426 **Materials**

427 1-palmitoyl-2-oleoyl-*sn*-phosphatidylcholine (PC), 1-palmitoyl-2-oleoyl-*sn*-
428 phosphatidylserine (PS), and cholesterol were purchased from Avanti Polar Lipids
429 (Alabaster, AL) as chloroform solutions (PC and PS) or powders (cholesterol). Cy3-
430 maleimide and Cy5-maleimide were purchased from GE Healthcare Life Sciences (Little
431 Chalfont, UK). n-octyl- β -D-glucoside (OG) was purchased from Dojindo (Kumamoto,
432 Japan). Monofunctional polyethylene glycol-succinimidyl valerate (s-PEG, 5000 mol wt)
433 and biotinylated monofunctional polyethylene glycol-succinimidyl valerate (b-PEG,
434 5000 mol wt) were purchased from Laysan Bio (Arab, AL). Chinese hamster ovary K1
435 (CHO-K1) cells were provided from RIKEN BRC through the National Bio-Resource
436 Project (MEXT, Tokyo, Japan).

437

438 **Plasmid construction**

439 Construction of the cDNA of full-length human EGFR (wt) fused with GFP was described
440 previously (14). T654A mutant DNA was constructed using PrimeSTAR Max (Takara,
441 Kusatsu, Japan) in the wt EGFR vector. The primer sequences were as follows:
442 EGFR(T654A)-f: GAAGCGCGCGCTGCGGAGGCTGCTGC and EGFR(T654A)-r:
443 CCGCAGCGCGCGCTTCCGAACGATGTG, respectively. For NanoBiT assays, full-
444 length human EGFR (wt or T654A mutant) was fused with LgBiT at the C-terminus (wt
445 or T654A EGFR-LgBiT), and GRB2 was fused with SmBiT at the N-terminus (GRB2-
446 SmBiT) as follows. The LgBiT fragment amplified from pBiT1.1-C [TK/LgBiT] Vector
447 (Promega) using KOD One PCR Master Mix (TOYOBO) was subcloned into the AgeI-
448 and NotI-digested EGFP-N1 vector (Clontech), and subsequently full-length EGFR
449 fragment was subcloned into the NheI- and HindIII-digested the LgBiT-inserted EGFP-
450 N1 vector. The GRB2-SmBiT fragment was constructed using KOD One PCR Master
451 Mix (TOYOBO), and subcloned into the AgeI- and SallI-digested EGFP-C2 vector
452 (Clontech). The primer sequence of SmBiT was designed from pBiT2.1-N [TK/SmBiT]
453 Vector (Promega).

454

455 **Peptide synthesis and purification**

456 Peptides corresponding to the TM-JM regions of EGFR (618-666) were synthesized by
457 solid-phase methods with the sequence KIPSIATGMV GALLLLLVALGIGLFM-
458 RRRHIVRKRT₆₅₄LRLLQERELVE-NH₂ (28). For the experiments with the C-terminal
459 labeled EGFR peptide, peptides containing a cysteine at the C-terminus were synthesized.
460 These synthetic peptides were purified by reverse-phase high-performance liquid

461 chromatography on a C4 column with a gradient of 1-propanol and acetonitrile (1:1) over
462 0.1% aqueous trifluoroacetic acid. To prepare the C-terminal labeled peptide, Cy3-
463 maleimide or Cy5-maleimide was introduced to the sulfide group on the cysteine at the
464 C-terminus of the TM-JM peptide by mixing the peptide and the fluorescence derivative
465 in dimethylformamide under basic conditions. For experiments with the N-terminal
466 labeled peptide, Cy3-COOH or Cy5-COOH was reacted with an elongating peptide on
467 the resin in the presence of 1-[bis(dimethylamino)methylene]-1H-benzotriazolium 3-
468 oxide hexafluorophosphate (HBTU) and diisopropylethylamine (DIEA), which activate
469 the carboxyl group on the fluorophore derivative. For synthesis of Thr654 phosphorylated
470 peptides, phosphorylated threonine derivatives were utilized. The purity was confirmed
471 by reverse-phase high-performance liquid chromatography and matrix-assisted laser-
472 desorption/ionization time-of-flight mass spectroscopy analysis.

473

474 **Nanodisc preparation**

475 For nanodisc construction, fluorescent EGFR TM-JM peptides co-solubilized with lipids
476 and OG in hexafluoroisopropanol were first dried to form thin films. These peptide films
477 were then resolubilized in buffer A (0.5 M NaCl, 20 mM Tris/Cl, 0.5 mM EDTA)
478 containing 30 mM OG and 5 mM dithiothreitol (pH 7.5). His8-tagged MSP 1E3D1 (MSP)
479 was expressed in *E. coli* and purified as described previously (41). The concentration of
480 MSP was quantified based on the absorbance at 280 nm ($29,910 \text{ M}^{-1}\text{cm}^{-1}$). Thin PC or PS
481 films were formed by evaporation of the solvent (chloroform) under a stream of nitrogen
482 gas and dried in vacuum. Cholesterol powders were first dissolved in chloroform, and a
483 thin film was formed as described above. PC, PS, and cholesterol were resuspended in
484 buffer A containing 0.4 M sodium cholate (pH 7.5) at a final concentration of 10 mM.
485 Cy3- and Cy5-labeled TM-JM peptides in buffer A were mixed in equal amounts and then
486 conjugated with MSP and phospholipid mixtures (PC, PC/PS, PC/cholesterol,
487 PC/PS/cholesterol) at a molar ratio of 1:1:120 μM (TM-JM/MSP/lipids). The mixture was
488 dialyzed against a buffer containing 0.5 M NaCl, 20 mM Tris/Cl, and 5 mM EDTA (pH
489 7.5) at 4°C to reconstitute the nanodiscs by removing the detergent. The aggregates and
490 liposomes were removed from the mixture by size-exclusion chromatography using a
491 Superdex 200 Increase column (GE Healthcare Life Sciences) and the peak fractions
492 containing nanodiscs of around 11 nm in diameter were collected.

493

494 **Single-pair FRET (spFRET) measurements**

495 Nanodisc samples were immobilized on the surface of a glass chamber as described
496 previously (20, 43, 44). Briefly, amine-modified glass surfaces were coated with 99% s-

497 PEG and 1% b-PEG. NeutrAvidin (Thermo Fisher Scientific, Waltham, MA) was then
498 bound to the b-PEG. The nanodisc samples bound with biotinylated anti-His8-tag
499 antibody (MBL Life Science) were loaded into the glass chamber and allowed to bind to
500 the NeutrAvidin-coated glass surface, after which unbound nanodiscs were washed away.
501 To reduce the photobleaching rate of Cy3 and Cy5, the nanodisc-loaded chamber was
502 filled with dialysis buffer containing 2-mercaptoethanol at the final concentration of 0.5%
503 (w/v). The fluorescence of Cy3 and Cy5 was observed under a TIRF microscope based
504 on an inverted microscope (Ti2; Nikon) with a 60x oil-immersion objective (ApoTIRF
505 60x 1.49 NA; Nikon). The fluorescence activity of Cy3 was excited using a 532 nm laser
506 (Compass 315M-100). Dual-color imaging was carried out through a 4x relay lens by
507 using two EMCCD cameras (C9100-134, ImagEM; Hamamatsu Photonics, Hamamatsu,
508 Japan) with a 200x EM gain. Images of 512 x 512 pixels (67 nm/pixel) were recorded
509 with a temporal resolution of 100 ms/frame using MetaMorph (Molecular Devices, San
510 Jose, CA) or AIS (ZIDO, Toyonaka, Japan).

511

512 **Analysis of FRET signals**

513 The measurement of fluorescence intensities of single nanodiscs was performed using
514 ImageJ software, as described previously (45). The background noise was filtered out
515 using the Subtract Background function in ImageJ. Fluorescence intensities of Cy3 and
516 Cy5 in single nanodiscs were measured as averages from circles with a diameter of 12
517 pixels containing a fluorescence spot. The average intensity of the same sized circles in
518 which no spot was present was subtracted as the background. Along the fluorescence
519 trajectories of TM-JM-Cy3 and TM-JM-Cy5, the FRET efficiency, E_{FRET} , for each frame
520 (> 2000) was calculated from the fluorescence intensities in the donor I_D and FRET I_A
521 channels as

$$522 \quad E_{FRET} = \frac{I_A - \beta I_D}{I_A + (\gamma - \beta) I_D},$$

523 where β and γ are coefficients for the compensation of fluorescence leakage from the
524 donor dye to the acceptor detector channel, and the difference in the detection efficiencies
525 of the dyes, respectively (46). Coefficients were calculated using the intensity time traces
526 as $\beta = 0.03$ and $\gamma = 0.4$, respectively. E_{FRET} distributions were all different in Kolmogorov-
527 Smirnov (KS) test with a rejection $p < 0.006$. The peak positions and their 95% percentile
528 section were estimated using bootstrap method from a discretized E_{FRET} distribution
529 (Table I), in which the bin width was set to 0.02 and the resampling number was 300. KS
530 test was done using “StatsKSTest” in Igor Pro 8.0 (WaveMetrix). Resampling for

531 bootstrap method was done using “sample” function in R.

532

533 **Cell culture and transfection**

534 CHO-K1 cells were maintained in HAM F12 medium supplemented with 10% fetal
535 bovine serum at 37°C under 5% CO₂. HEK293S cells were maintained in DMEM F12
536 medium supplemented with 10% fetal bovine serum at 37°C under 5% CO₂. For western
537 blotting assays, DNA constructs of full-length wt and T654A EGFR (1 µg) were
538 transiently transfected into CHO-K1 cells using FuGENE HD Transfection Reagent
539 (Promega, Madison, WI). For single-molecule measurements, CHO-K1 cells were
540 transfected with either a wt or T654A EGFR-GFP gene (0.5 µg each) using Lipofectamine
541 3000 Reagent (Thermo Fisher Scientific). For NanoBiT assays, HEK293S cells were
542 transfected with a mixture of wt or T654A EGFR-LgBiT gene (1 µg each) and GBR2-
543 SmBiT (0.2 µg) using Lipofectamine 3000 Reagent in 60 mm dish.

544

545 **PMA treatment and EGF stimulation**

546 DNA constructs of full-length wt and T654A EGFR were transfected and cultured with
547 10% fetal bovine serum (FBS) on the day before each measurement. Cells were then
548 starved in modified Eagle’s medium without FBS for 3 hours before the experiment.
549 Phorbol 12-myristate 13-acetate (PMA) was dissolved in DMSO and subsequently
550 diluted in PBS to a final concentration of 10 µM. For PMA pre-treatment, PMA solution
551 was added to the cell cultured medium at a final concentration of 100 nM and incubated
552 for 30 min at room temperature. For EGF stimulation, EGF (PeproTech, Cranbury, NJ)
553 dissolved in PBS was added to the cell cultured medium at a final concentration of 100
554 ng/mL (for western blotting assays and single-molecule measurements) or as a 0.001 to
555 100 nM dilution series (for the NanoBiT assay).

556

557 **Western blotting analysis**

558 In cells stimulated with EGF for 0, 5, 30 min at 37°C, threonine and tyrosine
559 phosphorylation of the wt and mutant T654A proteins was detected by western blotting
560 using rabbit anti-pT654 (ab75986; Abcam, Cambridge, UK) and rabbit anti-pY1086
561 antibody (#4407; Cell Signaling Technology, Danvers, MA), respectively. Rabbit anti-
562 EGFR antibody (#sc-03; Santa Cruz Biotechnology, Dallas, TX) was used to detect
563 protein expression. After being resolved by SDS-polyacrylamide gel electrophoresis
564 (PAGE), the electrophoresed proteins were transferred onto a polyvinylidene difluoride
565 (PVDF) membrane and incubated with each antibody (primary antibody) and then with a
566 horseradish peroxidase (HRP)-linked anti-rabbit IgG (secondary antibody; 7076, Cell

567 Signaling Technology). Immunoreactive proteins were detected with Amersham ECL
568 Prime Western Blotting Detection Reagent (GE Healthcare) using an ImageQuant LAS
569 500 device (GE Healthcare).

570

571 **Single-molecule imaging in living cells**

572 The methods for single-molecule measurement and analysis were described elsewhere
573 (Yanagawa and Sako, *Methods in Mol Biol*, in press; bioRxiv: doi:
574 10.1101/2020.06.08.141192). The single-molecule imaging of EGFR was performed at
575 the basal plasma membrane of the CHO-K1 cells at 25°C with the same microscopic
576 methods used for the spFRET measurements. The laser wavelength was 488 nm (Sapphire
577 488; Coherent, Santa Clara, CA) for the excitation of the GFP. Fluorescence images were
578 acquired every 50 ms using AIS software. The acquired multiple TIFF files were
579 processed by ImageJ software as follows: background subtraction was performed with a
580 rolling ball radius of 25 pixels, and two-frame averaging of the images was then
581 performed. Single-molecule tracking analysis was performed with AAS software (ZIDO).
582 All subsequent analyses were performed using smDynamicsAnalyzer
583 (<https://github.com/masataka-yanagawa/IgorPro8-smDynamicsAnalyzer>), an Igor Pro
584 8.0-based homemade program.

585

586 **NanoBiT assay**

587 HEK293S cells co-transfected with the plasmids of wt or T654A EGFR-LgBiT and
588 GRB2-SmBiT. Overnight after the transfection, cells were collected in 0.5 mM EDTA-
589 containing PBS, centrifuged, and suspended in 2 mL of HBSS containing 0.01 % bovine
590 serum albumin and 5 mM HEPES (pH 7.4) (assay buffer). The cell suspension was
591 dispensed in a 96-well white bottom plate at a volume of 80 μ L per well and loaded with
592 20 μ L of 25 μ M Nano-Glo Vivazine Live Cell Substrates (Promega) diluted in the assay
593 buffer. After incubation for 2 hrs at room temperature in the assay buffer, cells were
594 pretreated with PMA or vehicle as described above. Basal luminescence was then
595 measured by using a microplate reader (SpectraMax L, Molecular Devices) with an
596 interval of 60 sec at room temperature. After 10 min, 20 μ L of the EGF dilution series in
597 the assay buffer or the assay buffer (vehicle) were applied to each well using a benchtop
598 multi-pipetter (EDR-384SR, BioTec, Tokyo, Japan) under red dim light. Then,
599 luminescence was measured for 30 min with an interval of 60 sec. Each time-course of
600 luminescence counts was normalized with the luminescence counts of the vehicle-added
601 well. Dose-response curves were fitted with a Hill-equation to determine the maximum
602 intensity.

603 **Acknowledgments**

604 YS was supported by MEXT Japan with Grants-in-Aid for Scientific Research
605 (19H05647) and by JST CREST (JPMJCR1912). We thank Hiromi Sato for technical
606 assistance.

607

608 **Author contributions**

609 Conceptualization, R.M., Y.S.; methodology, R.M., T.S., M.Y., Y.S.; investigation, R.M.,
610 H. T., T. S., M.Y.; manuscript writing, R.M., T. S., Y.S. with feedback from all other
611 coauthors; funding acquisition, Y.S.; supervision, Y.S.

612

613 **Conflicts of interest**

614 None.

615

616 **References**

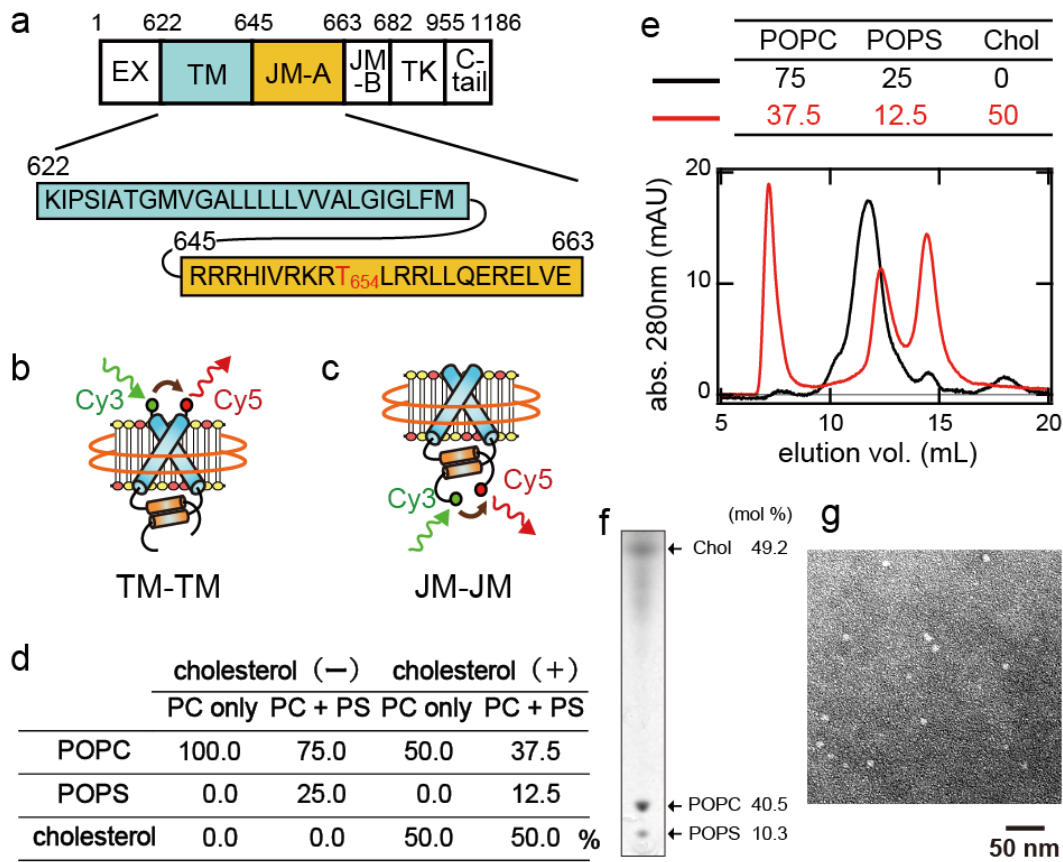
- 617 1. M. A. Olayioye, R. M. Neve, H. A. Lane, N. E. Hynes, The ErbB signaling network:
618 receptor heterodimerization in development and cancer. *EMBO J.* **19**, 3159-3167
619 (2000).
- 620 2. M. K. Nyati, M. A. Morgan, F. Y. Feng, T. S. Lawrence, Integration of EGFR inhibitors
621 with radiochemotherapy. *Nat. Rev. Cancer* **6**, 876-885 (2006).
- 622 3. E. Kovacs, J. A. Zorn, Y. Huang, T. Barros, J. Kuriyan, A structural perspective on the
623 regulation of the epidermal growth factor receptor. *Annu. Rev. Biochem.* **84**, 739-764
624 (2015).
- 625 4. N. J. Bessman, M. A. Lemmon, Finding the missing links in EGFR. *Nat. Struct. Mol.*
626 *Biol.* **19**, 1-3 (2012).
- 627 5. H. Ogiso *et al.*, Crystal structure of the complex of human epidermal growth factor and
628 receptor extracellular domains. *Cell* **110**, 775-787 (2002).
- 629 6. X. Zhang, J. Gureasko, K. Shen, P. A. Cole, J. Kuriyan, An allosteric mechanism for
630 activation of the kinase domain of epidermal growth factor receptor. *Cell* **125**, 1137-
631 1149 (2006).
- 632 7. M. J. Wagner, M. M. Stacey, B. A. Liu, T. Pawson, Molecular mechanisms of SH2- and
633 PTB-domain-containing proteins in receptor tyrosine kinase signaling. *Cold Spring*
634 *Harb Perspect Biol* **5**, a008987 (2013).
- 635 8. K. M. Ferguson *et al.*, EGF activates its receptor by removing interactions that
636 autoinhibit ectodomain dimerization. *Mol. Cell* **11**, 507-517 (2003).
- 637 9. N. F. Endres *et al.*, Conformational coupling across the plasma membrane in activation
638 of the EGF receptor. *Cell* **152**, 543-556 (2013).
- 639 10. E. R. Wood *et al.*, A unique structure for epidermal growth factor receptor bound to
640 GW572016 (Lapatinib): relationships among protein conformation, inhibitor off-rate,
641 and receptor activity in tumor cells. *Cancer Res.* **64**, 6652-6659 (2004).
- 642 11. N. Jura *et al.*, Mechanism for activation of the EGF receptor catalytic domain by the
643 juxtamembrane segment. *Cell* **137**, 1293-1307 (2009).
- 644 12. S. E. Webb *et al.*, Single-molecule imaging and fluorescence lifetime imaging microscopy
645 show different structures for high- and low-affinity epidermal growth factor receptors in
646 A431 cells. *Biophys. J.* **94**, 803-819 (2008).
- 647 13. Y. Huang *et al.*, Molecular basis for multimerization in the activation of the epidermal
648 growth factor receptor. *Elife* **5** (2016).
- 649 14. M. Hiroshima *et al.*, Transient Acceleration of Epidermal Growth Factor Receptor
650 Dynamics Produces Higher-Order Signaling Clusters. *J. Mol. Biol.* **430**, 1386-1401
651 (2018).

- 652 15. N. Jura, Y. Shan, X. Cao, D. E. Shaw, J. Kuriyan, Structural analysis of the catalytically
653 inactive kinase domain of the human EGF receptor 3. *Proc Natl Acad Sci U S A* **106**,
654 21608-21613 (2009).
- 655 16. S. J. Fleishman, J. Schlessinger, N. Ben-Tal, A putative molecular-activation switch in
656 the transmembrane domain of erbB2. *Proc Natl Acad Sci U S A* **99**, 15937-15940
657 (2002).
- 658 17. A. Arkhipov *et al.*, Architecture and membrane interactions of the EGF receptor. *Cell*
659 **152**, 557-569 (2013).
- 660 18. M. Lelimosin, V. Limongelli, M. S. Sansom, Conformational Changes in the Epidermal
661 Growth Factor Receptor: Role of the Transmembrane Domain Investigated by Coarse-
662 Grained MetaDynamics Free Energy Calculations. *J. Am. Chem. Soc.* **138**, 10611-10622
663 (2016).
- 664 19. C. Matsushita *et al.*, Transmembrane helix orientation influences membrane binding of
665 the intracellular juxtamembrane domain in Neu receptor peptides. *Proc Natl Acad Sci U*
666 *SA* **110**, 1646-1651 (2013).
- 667 20. R. Maeda, T. Sato, K. Okamoto, M. Yanagawa, Y. Sako, Lipid-Protein Interplay in
668 Dimerization of Juxtamembrane Domains of Epidermal Growth Factor Receptor.
669 *Biophys. J.* **114**, 893-903 (2018).
- 670 21. K. B. Abd Halim, H. Koldso, M. S. P. Sansom, Interactions of the EGFR juxtamembrane
671 domain with PIP2-containing lipid bilayers: Insights from multiscale molecular dynamics
672 simulations. *Biochim Biophys Acta* **1850**, 1017-1025 (2015).
- 673 22. Y. Wang *et al.*, Regulation of EGFR nanocluster formation by ionic protein-lipid
674 interaction. *Cell Res.* **24**, 959-976 (2014).
- 675 23. Y. Liu *et al.*, The involvement of lipid rafts in epidermal growth factor-induced
676 chemotaxis of breast cancer cells. *Mol. Membr. Biol.* **24**, 91-101 (2007).
- 677 24. T. Furuchi, R. G. Anderson, Cholesterol depletion of caveolae causes hyperactivation of
678 extracellular signal-related kinase (ERK). *J. Biol. Chem.* **273**, 21099-21104 (1998).
- 679 25. T. Ringerike, F. D. Blystad, F. O. Levy, I. H. Madshus, E. Stang, Cholesterol is
680 important in control of EGF receptor kinase activity but EGF receptors are not
681 concentrated in caveolae. *J. Cell Sci.* **115**, 1331-1340 (2002).
- 682 26. K. A. Lund *et al.*, Phosphorylation of the Epidermal Growth-Factor Receptor at
683 Threonine 654 Inhibits Ligand-Induced Internalization and down-Regulation. *J. Biol.*
684 *Chem.* **265**, 20517-20523 (1990).
- 685 27. M. Hiroshima *et al.*, Membrane cholesterol interferes with tyrosine phosphorylation but
686 facilitates the clustering and signal transduction of EGFR. *bioRxiv*
687 10.1101/2021.08.28.457965 (2021).

- 688 28. M. Hiroshima, Y. Saeki, M. Okada-Hatakeyama, Y. Sako, Dynamically varying
689 interactions between heregulin and ErbB proteins detected by single-molecule analysis
690 in living cells. *Proc Natl Acad Sci U S A* **109**, 13984-13989 (2012).
- 691 29. M. Yasui, M. Hiroshima, J. Kozuka, Y. Sako, M. Ueda, Automated single-molecule
692 imaging in living cells. *Nat Commun* **9**, 3061 (2018).
- 693 30. A. S. Dixon *et al.*, NanoLuc Complementation Reporter Optimized for Accurate
694 Measurement of Protein Interactions in Cells. *ACS Chem Biol* **11**, 400-408 (2016).
- 695 31. T. Sato, P. Pallavi, U. Golebiewska, S. McLaughlin, S. O. Smith, Structure of the
696 membrane reconstituted transmembrane-juxtamembrane peptide EGFR(622-660) and
697 its interaction with Ca²⁺/calmodulin. *Biochemistry* **45**, 12704-12714 (2006).
- 698 32. D. H. Jones, K. R. Barber, C. W. Grant, The EGF receptor transmembrane domain: 2H
699 NMR study of peptide phosphorylation effects in a bilayer environment. *Biochemistry*
700 **37**, 7504-7508 (1998).
- 701 33. K. Matsuzaki, Why and how are peptide-lipid interactions utilized for self-defense?
702 Magainins and tachyplesins as archetypes. *Biochim Biophys Acta* **1462**, 1-10 (1999).
- 703 34. M. Red Brewer *et al.*, The juxtamembrane region of the EGF receptor functions as an
704 activation domain. *Mol. Cell* **34**, 641-651 (2009).
- 705 35. X. Li, Y. Huang, J. Jiang, S. J. Frank, ERK-dependent threonine phosphorylation of EGF
706 receptor modulates receptor downregulation and signaling. *Cell. Signal.* **20**, 2145-2155
707 (2008).
- 708 36. H. J. Zhu, J. Iaria, S. Orchard, F. Walker, A. W. Burgess, Epidermal growth factor
709 receptor: association of extracellular domain negatively regulates intracellular kinase
710 activation in the absence of ligand. *Growth Factors* **21**, 15-30 (2003).
- 711 37. L. K. Goh, F. Huang, W. Kim, S. Gygi, A. Sorkin, Multiple mechanisms collectively
712 regulate clathrin-mediated endocytosis of the epidermal growth factor receptor. *J. Cell*
713 *Biol.* **189**, 871-883 (2010).
- 714 38. M. Kluba, Y. Engelborghs, J. Hofkens, H. Mizuno, Inhibition of Receptor Dimerization
715 as a Novel Negative Feedback Mechanism of EGFR Signaling. *PLoS One* **10**, e0139971
716 (2015).
- 717 39. K. Oda, Y. Matsuoka, A. Funahashi, H. Kitano, A comprehensive pathway map of
718 epidermal growth factor receptor signaling. *Mol. Syst. Biol.* **1**, 2005 0010 (2005).
- 719 40. S. Aifa *et al.*, Phosphorylation of Thr654 but not Thr669 within the juxtamembrane
720 domain of the EGF receptor inhibits calmodulin binding. *Biochem. Biophys. Res.*
721 *Commun.* **347**, 381-387 (2006).
- 722 41. K. Kojima, Y. Imamoto, R. Maeda, T. Yamashita, Y. Shichida, Rod visual pigment
723 optimizes active state to achieve efficient G protein activation as compared with cone

- 724 visual pigments. *J. Biol. Chem.* **289**, 5061-5073 (2014).
- 725 42. M. Wadsater, S. Maric, J. B. Simonsen, K. Mortensen, M. Cardenas, The effect of using
726 binary mixtures of zwitterionic and charged lipids on nanodisc formation and stability.
727 *Soft Matter* **9**, 2329-2337 (2013).
- 728 43. M. Pirchi *et al.*, Single-molecule fluorescence spectroscopy maps the folding landscape
729 of a large protein. *Nat Commun* **2**, 493 (2011).
- 730 44. R. Lamichhane *et al.*, Single-molecule view of basal activity and activation mechanisms
731 of the G protein-coupled receptor β_2 AR. *Proc. Natl. Acad. Sci. U. S. A.* **112**, 14254-
732 14259 (2015).
- 733 45. R. Maeda *et al.*, Single-molecule observation of the ligand-induced population shift of
734 rhodopsin, a G-protein-coupled receptor. *Biophys. J.* **106**, 915-924 (2014).
- 735 46. K. Okamoto, Y. Sako, Variational Bayes Analysis of a Photon-Based Hidden Markov
736 Model for Single-Molecule FRET Trajectories. *Biophys. J.* **103**, 1315-1324 (2012).
- 737

738 **Figures**

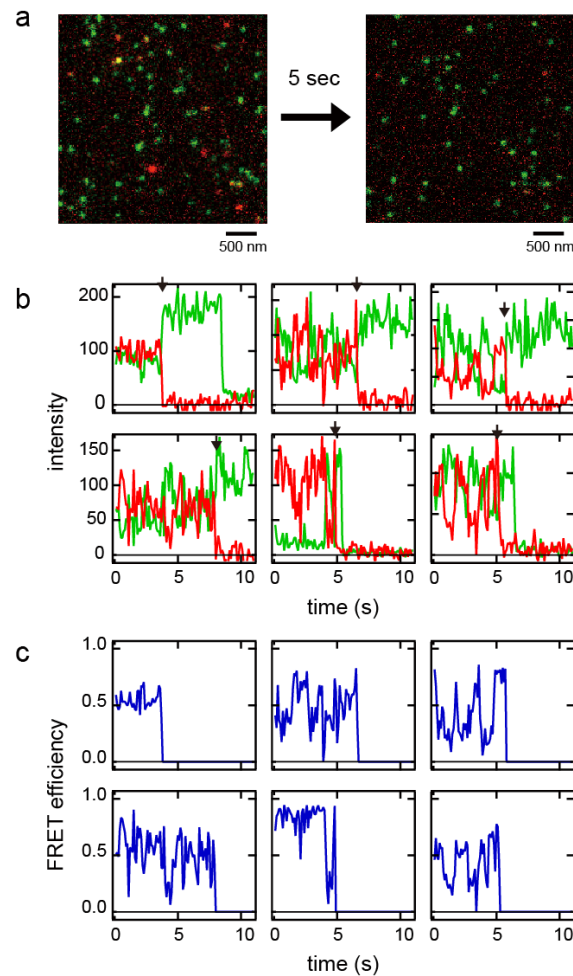


739

740 **Figure 1.** Construction of nanodiscs containing fluorescent TM-JM peptides of EGFR.
 741 (a) Amino acid sequence of the EGFR TM and JM-A domains. EX, extracellular domain;
 742 TK, tyrosine kinase domain. (b, c) Schematic images of nanodiscs containing dimeric
 743 TM-JM peptides fluorescently labeled at the N- (b) and C-terminus (c), respectively. (d)
 744 Lipid compositions used in the preparation of each nanodisc sample. The fractional ratios
 745 of PS and cholesterol mimic those in the mammalian plasma membranes. (e) Size-
 746 exclusion chromatography used for the purification of nanodiscs containing cholesterol
 747 (red) or not (black). The charge ratios of PC/PS/cholesterol are described in the upper
 748 table. The fraction having a peak absorbance of around 12 elution volumes (mL) was
 749 collected and used for the subsequent experiments. (f) Thin-layer chromatography of the
 750 nanodisc fraction containing cholesterol (fraction 12 in (e)). (g) A negative stain electron
 751 micrograph of fraction 12 in (e). Size distribution of the nanodiscs calculated from the
 752 images was fitted with a Gaussian function, with a mean diameter of 11 ± 2 nm.

753

754

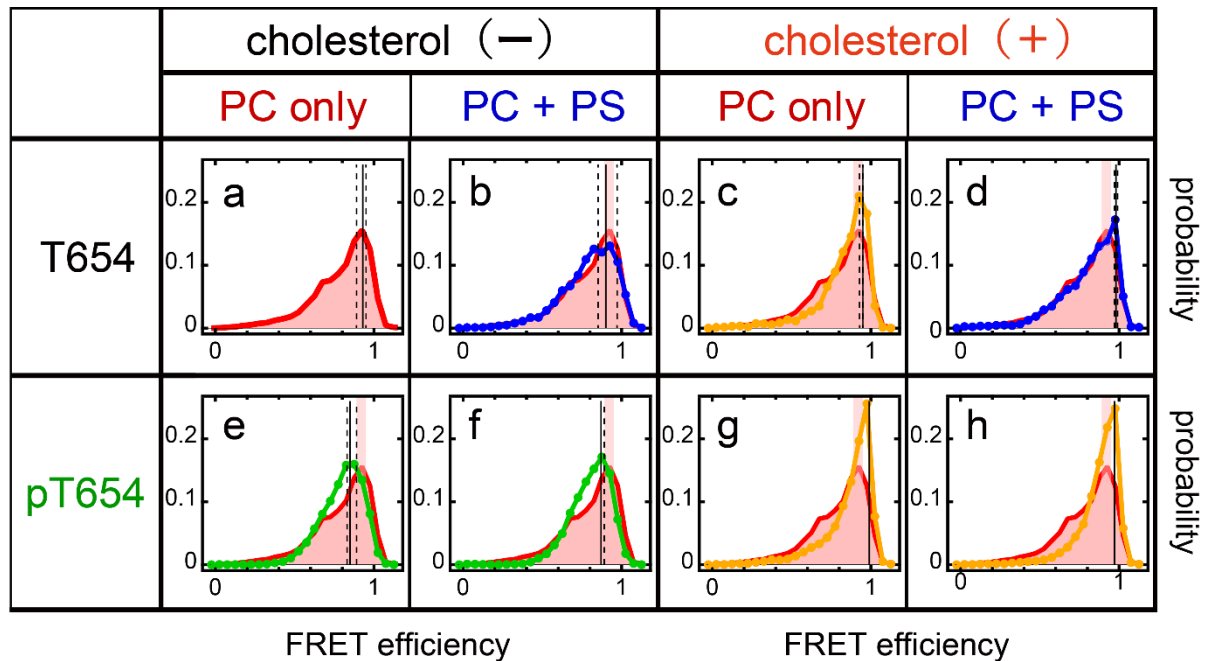


755

756 **Figure 2.** Single-pair FRET measurement of the EGFR TM-JM dimers in nanodiscs. (a)
757 Fluorescence micrograph of nanodiscs illuminated with a green laser. Cy3 (green) and
758 Cy5 (red) emissions were superimposed. The Cy5 emission was caused by FRET from
759 Cy3. (b) Representative fluorescence trajectories of Cy3 (green) and Cy5 (red). Black
760 arrows indicate photobleaching points of Cy5. (c) FRET efficiency trajectories of the
761 fluorescence trajectories in (b). The FRET efficiency, E_{FRET} , was calculated as described
762 in the Materials and Methods section. Typical fluorescence and FRET trajectories
763 between peptides labeled at the C-terminus are shown. Transitions to low FRET
764 efficiency states suggested that dissociation of the JM dimer occurred occasionally. The
765 Förster radius R_0 between Cy3 and Cy5 is 5.6 nm.

766

767

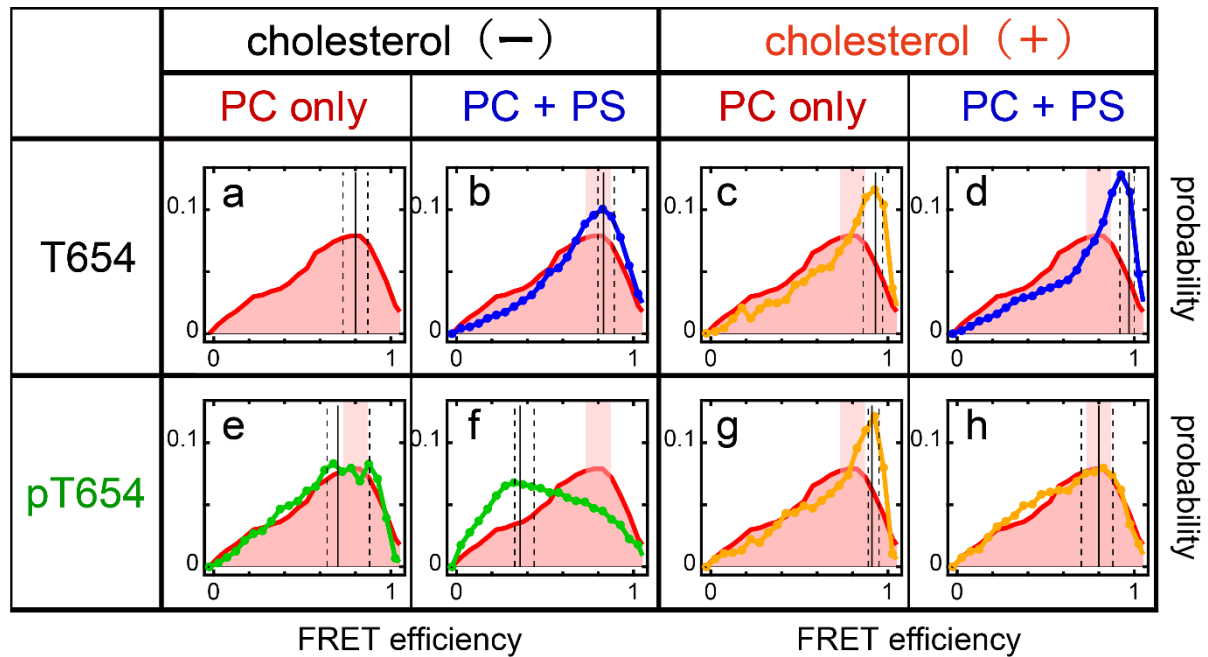


768

769 **Figure 3.** FRET efficiency (E_{FRET}) distributions in nanodiscs containing a single
770 Cy3/Cy5-pair of N-terminal labeled peptides. Nanodiscs contained non-phosphorylated
771 (a–d) and Thr654 phosphorylated (e–h) peptides at the indicated lipid conditions.
772 Positions of the mode and its 5-95% percentile section are indicated by solid and dashed
773 lines, respectively. See Table I for these values. In (b–h), the distribution and the 95%
774 percentile section shown in (a) are superimposed (red) for comparison.

775

776

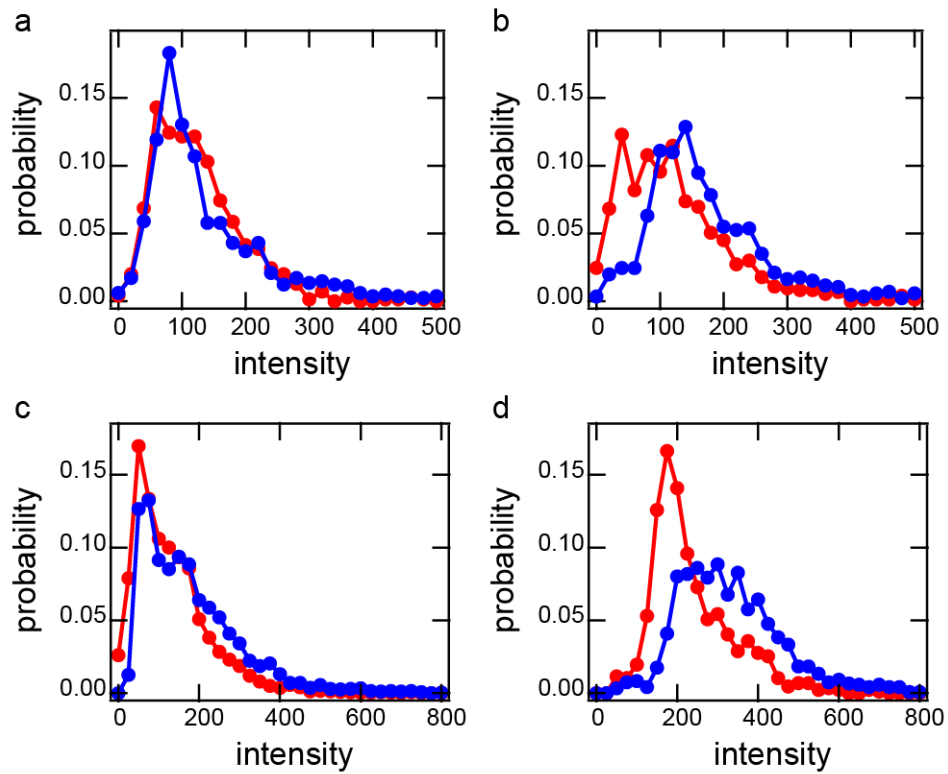


777

778 **Figure 4.** E_{FRET} distributions in nanodiscs containing a single Cy3/Cy5-pair of C-terminal
 779 labeled peptides. Nanodiscs contained non-phosphorylated (a–d) and Thr654
 780 phosphorylated (e–h) peptides in the indicated lipid conditions. Positions of the mode and
 781 its 5-95% percentile section are indicated by solid and dashed lines, respectively. See
 782 Table I for these values. In (b–h), the distribution and the 95% percentile section shown
 783 in (a) are superimposed (red) for comparison.

784

785



786

787 **Figure 5.** Higher-order oligomerization of EGFR TM-JM peptides in the nanodiscs.

788 Histograms are shown of the total fluorescence intensity of the peptides with Cy3-labeling

789 at the C-terminus in single nanodiscs containing cholesterol (blue) or not (red). Discs

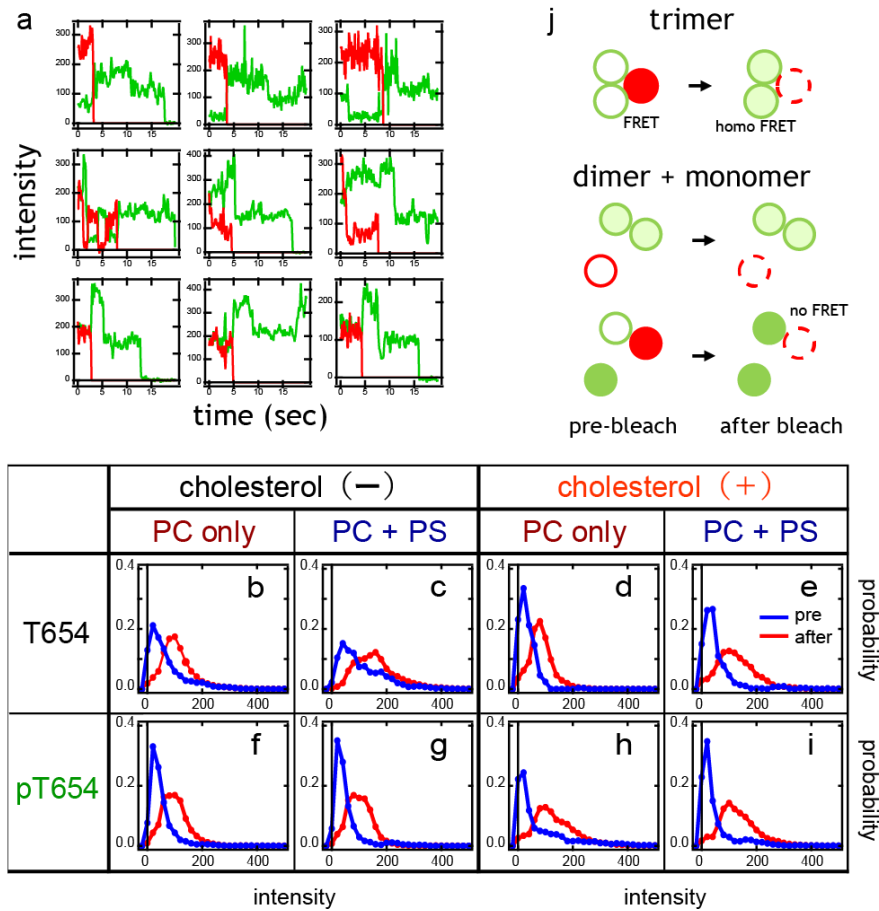
790 containing no Cy5 peptide were chosen for measurement to avoid the possible effects of

791 FRET. Peptides with a non-phosphorylated (**a, c**) or phosphorylated (**b, d**) Thr654 were

792 reconstituted into nanodiscs in PC (**a, b**) or PC/PS (**c, d**) membranes.

793

794

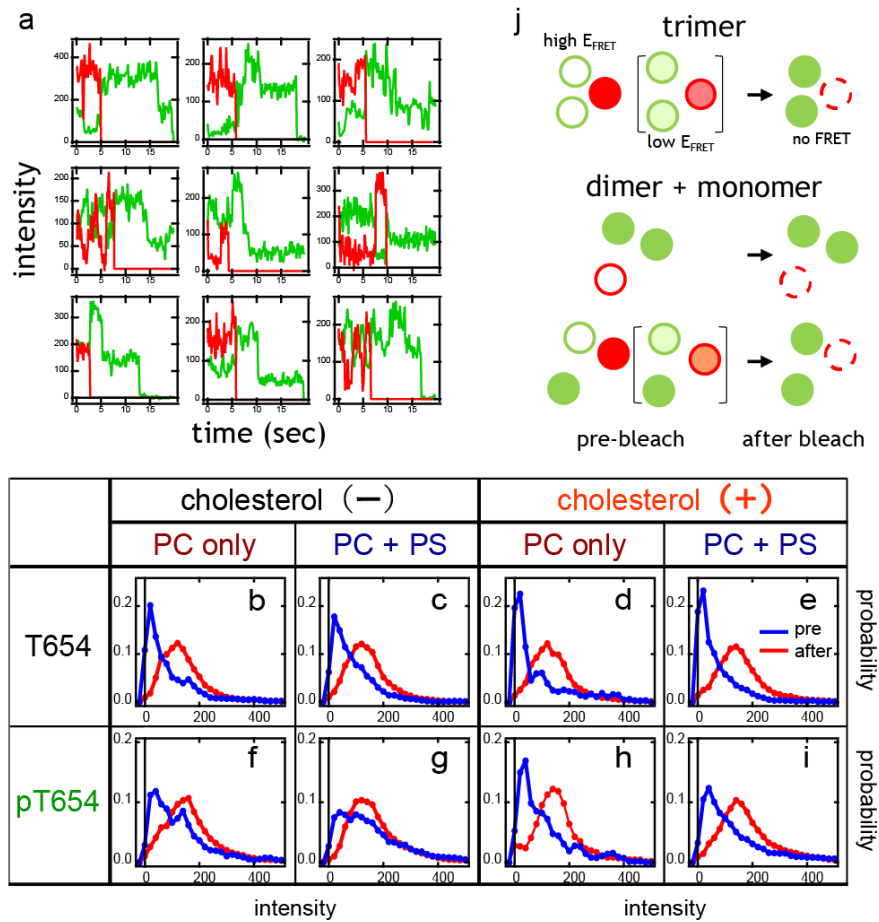


795

796 **Figure 6.** Assembly of EGFR TM regions. **(a)** Representative fluorescence trajectories of
 797 Cy3 (green) and Cy5 (red) in nanodiscs containing two Cy3-labeled and one Cy5-labeled
 798 peptide. Fluorescence intensities and/or two-step photobleaching dynamics after Cy5
 799 photobleaching indicated that these nanodiscs contained two Cy3 peptides. **(b–i)**
 800 Fluorescence intensity histograms of N-terminal-labeled Cy3 peptides before (blue) and
 801 after (red) Cy5 photobleaching. Nanodiscs contained non-phosphorylated **(b–e)** and
 802 Thr654 phosphorylated **(f–i)** peptides at the indicated lipid conditions. **(j)** Schematic
 803 structures indicating proximity between three TM domains before (left) and after (right)
 804 Cy5 photobleaching. Note that acceptance of the excitation energy from Cy3 was not
 805 saturated for Cy5 under our experimental conditions, even in the presence of two Cy3
 806 molecules.

807

808

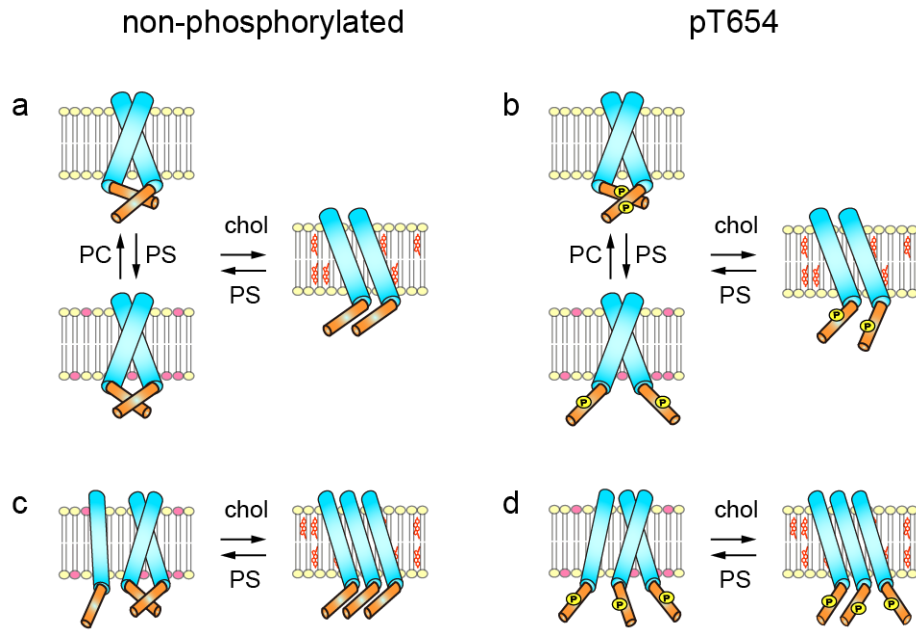


809

810 **Figure 7.** Assembly of EGFR JM regions. **(a)** Representative fluorescence trajectories of
 811 Cy3 (green) and Cy5 (red) in nanodiscs containing two Cy3-labeled and one Cy5-labeled
 812 peptide at the C-terminus. **(b–i)** Fluorescence intensity histograms of C-terminal-labeled
 813 Cy3 peptides from nanodiscs containing two Cy3 and one Cy5 peptide before (blue) and
 814 after (red) Cy5 photobleaching. Nanodiscs contained non-phosphorylated **(b–e)** and
 815 Thr654 phosphorylated **(f–i)** peptides at the indicated lipid conditions. **(j)** Schematic
 816 structures indicating proximity between three JM domains before (left and middle) and
 817 after (right) Cy5 photobleaching.

818

819

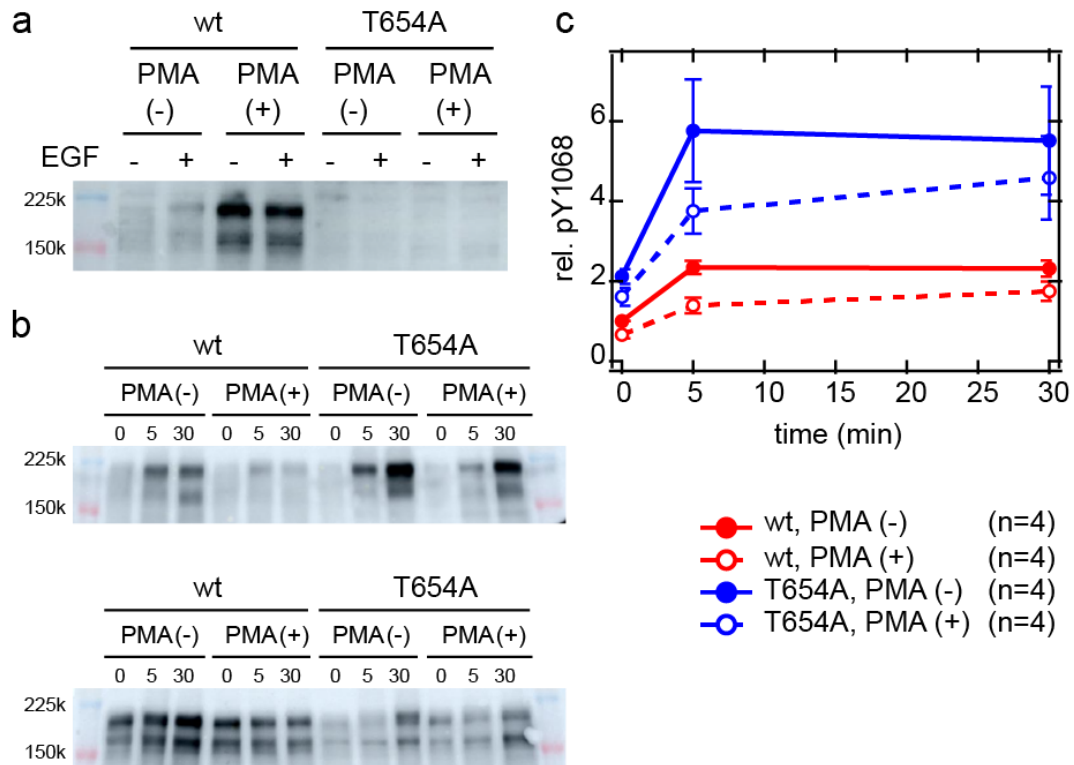


820

821 **Figure 8.** Possible configurations of EGFR TM-JM dimers and trimers regulated by
822 membrane lipids and Thr654 phosphorylation.

823

824

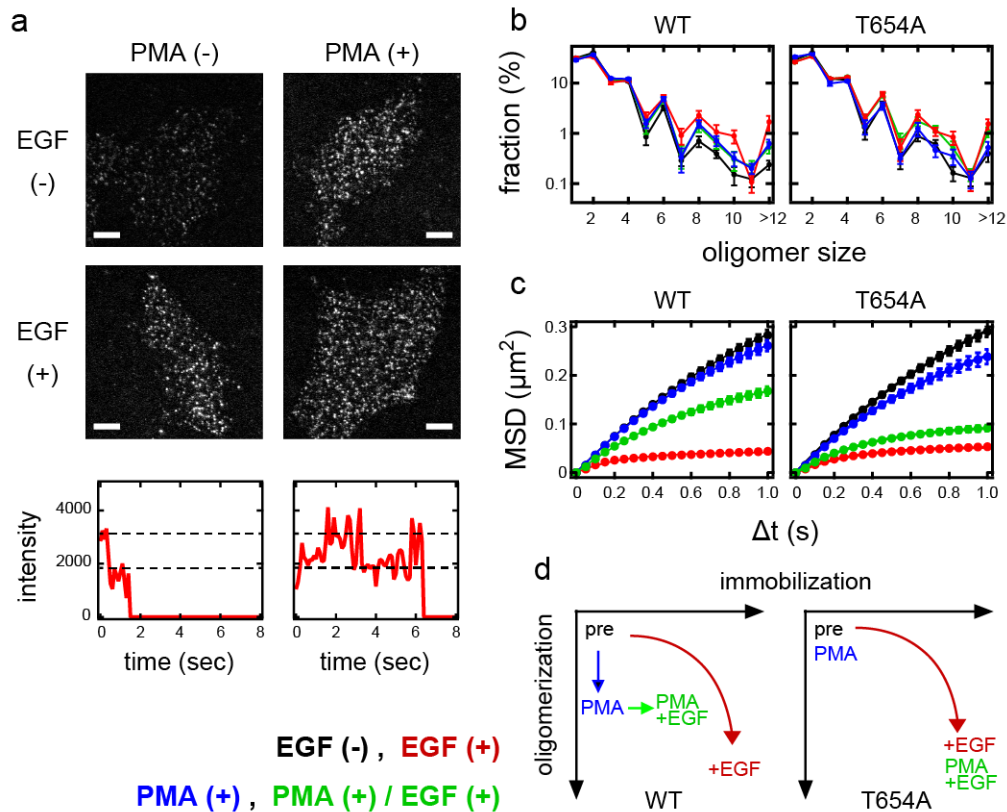


825

826 **Figure 9.** Thr and Tyr phosphorylation of EGFR. **(a)** Thr654 phosphorylation after EGF
 827 stimulation and PMA pretreatment. **(b, c)** Timecourses of Y1068 phosphorylation for the
 828 wt and T654A mutant of EGFR during EGF stimulation. Typical western blotting results
 829 are indicated **(b, top)** and the average of four independent experiments are shown with
 830 SE **(c)**. Phosphorylation levels were normalized to the expression levels of the whole
 831 EGFR molecule **(b, bottom)**.

832

833



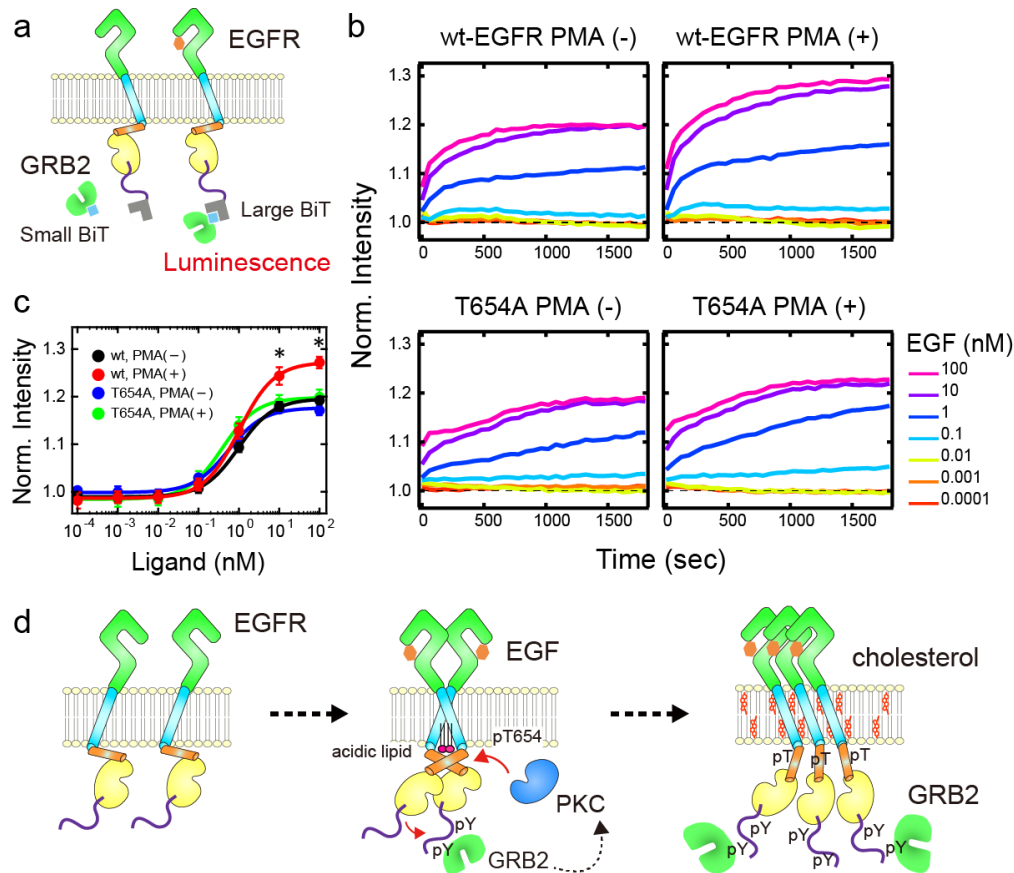
834

835 **Figure 10.** Oligomerization and lateral movements of EGFR on the living cell surface.
 836 (a) Single molecule imaging of wt EGFR-GFP on the surface of living CHO-K1 cells
 837 with (right) and without (left) PMA pretreatment. Cells were stimulated with (lower) and
 838 without (upper) EGF. Bar, 5 μm . Quantized transitions in the fluorescence intensities
 839 (bottom) indicate single-molecule resolution of the imaging. (b) Oligomer size
 840 distributions of wt (left) and T654A mutant (right) EGFR in cells. The oligomer size ratio
 841 was measured before and 10 min after EGF stimulation. (c) Mean square displacement
 842 (MSD) of wt (left) and T654A (right) EGFR spots as a function of the time interval,
 843 indicating lateral mobility. The MSD was calculated before and 10 min after EGF
 844 stimulation. In (b, c), cells were pretreated with (blue, green) or without (black, red) PMA
 845 and stimulated (red, green) or not (black, blue) with EGF. (d) Diagram of the
 846 oligomerization and immobilization states of wt (left) and T654A mutant (right) EGFR
 847 suggested from single-molecule measurements. Arrows indicate the state transitions after
 848 PMA treatment and EGF stimulation.

849

850

851



852

853 **Figure 11.** NanoBiT assay for the EGFR/GRB2 interaction in living cells. (a) Schematic
 854 illustration of the NanoBiT assay of EGFR/GRB2 interactions. (b) Typical time courses
 855 of chemiluminescence signals generated from the complex formation of large BiT
 856 (LgBiT)-fused EGFR and small BiT (SmBiT)-fused GRB2 after EGF application at time
 857 0. The final concentration of EGF in the culture medium was varied from 0.0001 to 100
 858 nM. Measurements were done in cells with (+) or without (-) PMA pretreatment. (c) Dose
 859 dependency of the chemiluminescence intensities at 30 min after EGF stimulation. The
 860 average values from four independent experiments are shown with SE. Lines indicate
 861 fitting with a Hill-equation function. * $p < 0.05$ determined by t -test against the signal in
 862 wt cells without PMA. (d) A schematic model of the activation and signal transduction
 863 process for EGFR dimers and oligomers. In the oligomers of EGFR, affinity with GRB₂
 864 is increased.

865

866

867 **Table I. Peak values in the E_{FRET} distributions between the TM-JM peptides**

868

lipid composition	pT654	labelling			
		N-term		C-term	
		mean	95%	mean	95%
PC	-	0.93	(0.89-0.95)	0.81	(0.73-0.87)
PC/PS	-	0.90	(0.85-0.97)	0.83	(0.79-0.89)
PC/chol	-	0.95	(0.93-0.95)	0.93	(0.85-0.97)
PC/PS/chol	-	0.98	(0.97-0.99)	0.94	(0.91-0.97)
PC	+	0.85	(0.83-0.89)	0.68	(0.63-0.89)
PC/PS	+	0.87	(0.87-0.89)	0.36	(0.33-0.43)
PC/chol	+	0.99	(0.99)	0.90	(0.89-0.95)
PC/PS/chol	+	0.97	(0.97)	0.82	(0.81-0.89)

869

870

871 Mean and their 95% percentile section of the peak values in Figs 3 and 4 were estimated
872 by bootstrap method with 300-times of resampling. An increase of the resampling times
873 to 1000 did not change the result.